

**An Experimental Investigation of Load Cell Wall
Response to Quasi-Static and Impact Loading when
using an Aluminium Honeycomb Barrier Face**

By Dr H C Davies

PPR133

PUBLISHED PROJECT REPORT

TRL Limited



PUBLISHED PROJECT REPORT PPR133

An Experimental Investigation of Load Cell Wall Response to Quasi-Static and Impact Loading when using an Aluminium Honeycomb Barrier Face

Version: Final

by Dr H C Davies (TRL Limited)

Prepared for: Project Record: Load Cell Wall
Client: Dr R M Kimber (Science and Engineering Director)
Transport Research Foundation

Copyright TRF Limited July 2006

This report has been prepared for the Transport Research Foundation. The views expressed are those of the author(s) and not necessarily those of the Transport Research Foundation.

Approvals	
Project Manager	Dr Huw Davies
Quality Reviewed	Dr Mervyn Edwards

This report has been produced by TRL Limited, under/as part of a Contract placed by the Transport Research Foundation. Any views expressed are not necessarily those of the Transport Research Foundation.

TRL is committed to optimising energy efficiency, reducing waste and promoting recycling and re-use. In support of these environmental goals, this report has been printed on recycled paper, comprising 100% post-consumer waste, manufactured using a TCF (totally chlorine free) process.

CONTENTS

1	Introduction	2
2	Aluminium Honeycomb Core	3
3	Experimental Study	4
3.1	Results and Discussion	6
3.1.1	Uniform crush tests	6
3.1.2	Penetration – Fixed load area	10
3.1.3	Penetration – Increasing load area	12
4	Mathematical Modelling	13
4.1	Preliminary Assessment	13
4.1.1	Continuous mesh model	13
4.1.2	Discrete mesh model	15
4.1.3	Model comparison	16
4.2	Discrete Mesh Honeycomb Assessment	17
4.2.1	Model characteristics	17
4.2.2	Model development	21
4.2.3	Results and discussion	22
5	Conclusions	32
5.1	Experimental Study	32
5.2	Mathematical Simulation	33
	Acknowledgements	35

Executive Summary

A possible method for assessing vehicle crashworthiness involves crashing the vehicle into a load cell wall faced with aluminium honeycomb. Optimisation of this approach requires an understanding of the force transmission characteristics of aluminium honeycomb structures. This experimental investigation considered the change in load cell wall response to quasi-static and dynamic impact loads when applied through an aluminium honeycomb barrier face.

Quasi-static crush and dynamic impact experiments were used to investigate force transmission characteristics for three types of aluminium honeycomb. Three different loading configurations were used to replicate the aluminium honeycomb deformation observed in car-to-barrier tests. These were uniform crush (out-of-plane loading of the aluminium honeycomb), penetration with a fixed load area (out-of-plane and shear loading) and penetration with an increasing in load area (out-of-plane, in-plane and shear loading). Key findings were that force level is affected by loading rate (up to a 40% increase at the maximum 15m/s test speed was measured) and by penetration tearing the of the aluminium honeycomb cell walls (tear forces of between 0.9kN/m to 4.0kN/m were recorded), whilst force distribution is affected by relative density and depth of the aluminium honeycomb (increased load spread). Other important findings were that pre-crushing removed an initial peak in the force level when subject to quasi-static loading and reduced this peak when subject to dynamic loading (the difference due to inertia of the honeycomb material in dynamic tests). However, increasing the pre-crush beyond 1-2mm increased resistance to penetration and increased peak load and load spread (the stiffer pre-crushed layer created a sandwich structure in which the stiffer pre-crushed layer spread the load over the less stiff uncrushed layer). The addition of in-plane loading resulted in force redistribution (due to rotation/buckling of the aluminium honeycomb) and reduction in force level (due to fracture of the aluminium honeycomb).

Another approach to assessing crashworthiness is to use numerical simulation (finite element modelling). Mathematical simulation is a powerful tool that enables studies with many parameters and large modifications. Two approaches to finite element modelling of aluminium honeycomb were investigated. The investigation was based on the ability of the model to predict force transmission consistent with the results of the experimental study. A continuous mesh approach was found not to replicate the localised penetration observed in the experimental study, resulting in a significant increase in force level and distribution. A discrete mesh approach allowed localised penetration of the honeycomb to be modelled without the large distortion of the surrounding material and consistent with the experimental study. However, the mesh density was too coarse to be able to reliably predict the force levels and distributions found in the experimental study. Aluminium honeycomb can shear at the junction between each cell, whilst this is limited to the break between each column in the model (the cell density for the aluminium honeycomb was far higher than the column density for the honeycomb model). Increasing the column density resulted in the HC model becoming unstable. Unlike a continuous mesh model, in which individual columns stabilise neighbouring columns, relative movement of columns is possible in the discrete mesh model. This places greater emphasis on individual column stability. Column stability was shown to be dependent on loading condition, slenderness ratio (column area relative to height) and the honeycomb element stress/strain profile.

1 Introduction

Since the introduction of the European Frontal and Side Impact Directives in October 1998 (United Nations Regulation 94), most manufacturers and governmental bodies now recognise that vehicle crash compatibility offers the next greatest potential benefit for improving car occupant safety and reducing road casualties. Indeed, addressing frontal impact compatibility is essential if the improvements in car secondary safety are to be fully realised in accidents on the road and future advanced restraint systems are to be effective.

As part of the proposed assessment of vehicle crash compatibility, a full width impact test in conjunction with a load cell wall (LCW) to measure and control the car's frontal force distribution is proposed (Davies *et al.* 2004). The logic behind this test is that cars with a more homogeneous frontal force distribution should offer greater structural interaction potential; structural interaction being an essential prerequisite for improved crash compatibility. Optimisation of this approach requires an understanding of the force transmission characteristics of aluminium honeycomb structures.

The most oft quoted study looking at crush behaviour of honeycomb core is that by McFarland (1963), who developed a semi-empirical model to predict crushing stress of hexagonal cell structures subject to axial loading. Later research, such as that by Gibson and Ashby (1988), builds upon this earlier work by considering both bending and extension deformation, and taking into account mechanical properties in both ribbon and expansion directions. The need to consider both ribbon and expansion directions is due to the fact that aluminium honeycomb cellular structure is anisotropic. Very few of the published studies consider dynamic crushing behaviour or response to penetration of aluminium honeycomb cellular structures. Notable exceptions are studies by Wu and Wu-Shung (1996), and Zhao and Gary (1998), who have reported on experimental work looking at crushing phenomena of aluminium honeycomb cellular structures under both quasi-static and impact loading conditions, and Goldsmith *et al* (1992; 1995) who reported on the results of experimental work on both quasi-static and dynamic penetration of aluminium honeycomb cores. However, none of the above studies undertook to investigate force transmission, although factors that may well influence force transmission have been identified in the discussions.

This report discusses the results of experimental investigations of force transmission of aluminium honeycomb structures under both quasi-static and dynamic impact loading conditions, where the direction of the applied load is along the cell axis and the loading area is large in comparison to the cross-section of an individual cell. Three types of aluminium honeycombs were evaluated using three basic loading patterns. As the automotive industry increasingly uses numerical crash simulation – due to cost and time considerations – an evaluation of two approaches to modelling aluminium HC is also discussed.

2 Aluminium Honeycomb Core

Aluminium honeycombs are manufactured by bonding together sheets of aluminium foil, which are then expanded to form a cellular honeycomb configuration. The hexagonal core as used in vehicle crash test barrier faces is the most basic and common cellular configuration (Figure 1); the T direction is along the cell axis and is referred to as the primary direction, the L direction as the ribbon direction, the W direction as the expansion direction. Used as a barrier face, the orientation is such that the T direction of the core is aligned with the direction of travel of the vehicle.

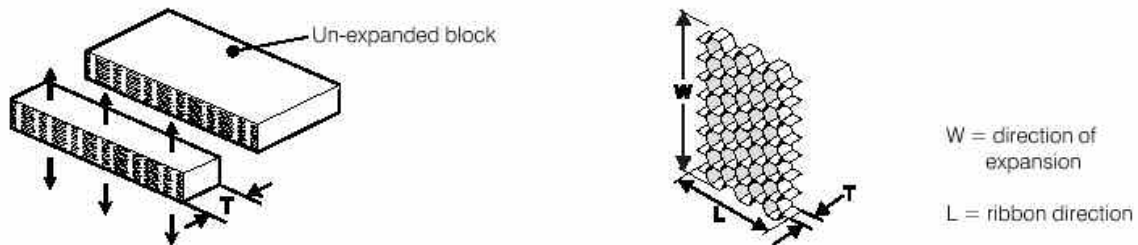


Figure 1: Hexagonal aluminium honeycomb core.

The axial compressive strength of the honeycomb is highest in the T direction and is characterised by a sharply rising peak – the linear-elastic deformation stage – prior to longer plateau – the plastic deformation stage. The peak is often referred to as the ‘bare compressive strength’ and the plateau the ‘crush strength’ (Figure 2). The plateau region manifests a series of oscillations which depict the successive plastic buckling of the cell walls in an accordion fashion. When used as an energy absorber, the core is often pre-crushed slightly to remove the initial elastic compressive peak in the load deflection curve. Eventually at high strains the cells will collapse sufficiently so that the cell walls touch, further deformation compresses the cell material itself. This gives a steep rising portion of the stress-strain curve referred to as ‘densification’.

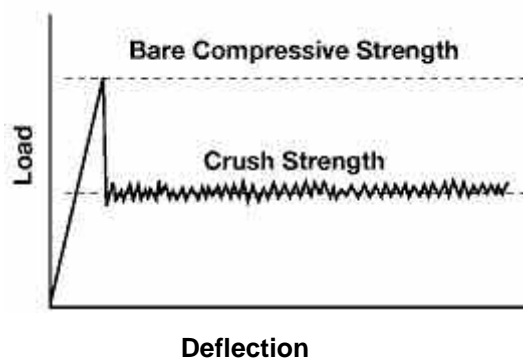


Figure 2: Typical load deflection curve for aluminium honeycomb showing the difference between the bare compressive strength and the crush strength.

For the L and W directions the compressive strength is much less – typically less than 5% of the crush strength in the T direction – and the load deflection curves exclude the initial high elastic compressive peak observed in the T direction prior to the onset of plastic deformation. This is due to the fact that the stresses in the L and W directions make the cell walls bend, whilst in the T direction they require axial compression of the cell walls. As with compressive strength, the shear strength of aluminium honeycomb core varies significantly with loading plane, being far higher in the LT and WT planes than for the LW plane.

3 Experimental Study

The experimental study aimed to assess the effect of using aluminium honeycomb core as a barrier face upon load cell wall measured load and load distribution when subject to quasi-static and impact (dynamic) loading. Load was applied to the front face of an aluminium honeycomb block of known characteristics in one of three basic configurations and measured by a load cell wall of resolution 125mm x 125mm.

In total, three types of aluminium honeycomb core were considered in the experimental investigation; two of these were to the same specification as those used in the ECE R94 impact test (United Nations Regulation 94), the third approximately midway between the other two in terms of crush strength in the T axis. The core designation and crush strength* in the T axis as supplied by the manufacturer were as follows:

Cell Size (Inches) – Aluminium Alloy – Foil Thickness† (Inches) – Density‡ (lbs/ft³)

3/4 – 3003 – 0.003 – 1.8 (crush strength 0.34MPa +/-10%)

3/8 – 3003 – 0.003 – 3.7 (crush strength 1.02MPa +/-10%)

1/4 – 3003 – 0.003 – 5.2 (crush strength 1.71MPa +/-10%)

Conversion Factors

Length: 1 Inch = 25.4 mm

Density: 1 lbs/ft³ = 16.02 kg/m³

The crush strength of the aluminium honeycomb is related to the relative density based on the following equation (Wierzbicki, 1983):

$$\frac{(\sigma_{pl})_T}{\sigma_{ys}} = 6.6 \left(\frac{t}{l} \right)^{5/3}$$

Where σ_{pl} and σ_{ys} are the plastic collapse stress of the aluminium honeycomb in the T direction and yield stress of the aluminium material respectively, and $\frac{t}{l}$ is the relative density (dependent on foil thickness and cell size). For the range of cores investigated, this equation predicts an increase in crush stress by a factor of 6, this compares well with the actual increase in crush stress (0.34MPa to 1.71MPa) when allowance is made for the crush stress tolerance of +/-10%.

As foil grade and foil thickness were the same for each sample, these values are omitted when referencing the different cores. The sizes for each specimen are given in the format L x W x T, unless otherwise stated. When calculating crush strength in the T direction, the block surface area was based on the contribution of complete cells only. This was to minimise the effect of broken (incomplete) cells around the edges of the block.

For the quasi-static loading experiments a Losenhausen 600 tonne hydraulic press was used to apply load to the front face of an aluminium honeycomb block. The load was recorded by nine load cells arranged in a 3 x 3 matrix behind the aluminium honeycomb block. A displacement transducer was

* The core is chemically etched to achieve the required crush stress tolerance

† Measured to the nearest 0.001"

‡ Density has a variation of +/-17% for commercial grade core

attached to the side of the hydraulic press to record the displacement of the loading face relative to the platen on which the load cells were placed. A Prosig Conquest data acquisition device was used to record the output from the nine load cell channels in addition to that of the displacement transducer. The experiments were carried out at a position control rate of approximately 0.5mm/s and the data sampled at 1Hz. Prior to the tests, the heights of the load cells were adjusted using shims in order to ensure a flat loading surface^{*}; the honeycomb core acts as a rigid block prior to any crush initiation due to its high shear strength in the LT and WT planes, hence any local high points on the load cell wall surface would act as a focal points for the applied load.

For the dynamic loading experiments, the helmet drop test rig at TRL was used. This rig uses two vertical wires that are spaced 480mm apart to guide a falling projectile of up to 15kg onto a target at up to 15m/s. In these experiments, the target was either a single load cell, or nine load cells arranged in a 3 x 3 matrix, both faced with aluminium honeycomb blocks. A transducer mounted onto the projectile was used to measure acceleration and a Prosig Conquest data acquisition device recorded the output from the load cell channels. The data was subsequently filtered at CFC1000[†] to remove any underlying high frequencies. Each of the load cells was bolted to a back plate with a torque of 40Nm[‡], to prevent any resonance occurring. As with the quasi-static loading, the heights of the load cells were adjusted using shims in order to ensure a flat loading surface.

Three different load configurations were assessed as part of this research. The direction of the applied load in each case aligned with the T direction of the honeycomb core – the T direction of the honeycomb core normal to the load cell wall surface. The different load configurations are detailed below:

- Uniform load distribution over the front face of the aluminium honeycomb core, the honeycomb core block having frontal area of either 125mm x 125mm or 375mm x 375mm. This would promote failure of the core in axial crush.
- Fixed load area of 125mm x 125mm, the front face of the honeycomb block having a front area of 375mm x 375mm. The intention was to promote penetration of the honeycomb core as observed in the vehicle impact tests and understand the influence of core shear strength upon load cell wall measured load and load distribution (Figure 3).



^{*} Average cell-to-cell height tolerance of the LCW was measured at 0.34mm prior to shimming

[†] Indicates that the frequency response lies within specified limits (ISO 6487)

[‡] Manufacturer specified torque setting – verified by experimental testing

Figure 3: Dynamic penetration test set-up with the impactor aligned with the centre load cell of the 3 x 3 load cell matrix.

- Linear increase in load area in either ribbon or expansion directions. This was achieved using a wedge with the two faces angled at 45° from the front face of the honeycomb (Figure 4). The intention was to promote crush in both the primary and the ribbon/expansion direction, such deformation being a feature of barrier deformation noted in vehicle impact tests.



Figure 4: Quasi-static wedge test.

The chosen test configurations aimed to provide insight into the force transmission characteristics of aluminium honeycomb structures pertinent to vehicle crash testing.

3.1 Results and Discussion

3.1.1 Uniform crush tests

Quasi-static crush strength of the different core types was observed to be dependent on the proportion of edge columns within the test piece. A proportion greater than 20% resulted in crush strength below that quoted by the manufacturer. This was due to the fact that these columns failed differently from those within the block, displaying a more irregular folding as a consequence of the differences in stress concentration around the column edge. In addition, for those test pieces with a high slenderness ratio, irregular folding of the outer columns can induce bending moments in the block leading to buckling failure and further reduction in compressive strength (Figure 5). This ‘edge effect’ has been previously documented in an previous TRL study and a value has been estimated for those core types tested. A similar estimation was not performed for this experimental study due to the buckling failure observed for some of the test pieces.

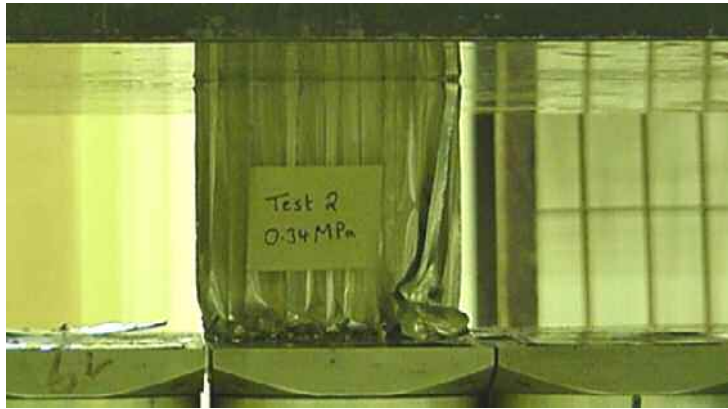


Figure 5: Quasi-static loading of a 3/4-1.8 aluminium honeycomb test piece highlighting failure in buckling of one of the edge columns.

This ‘edge effect’ is at odds with a study conducted by Wu and Wu-Shung (1996) who found no discernable effect on crush strength with changes in column numbers. The study by Wu and Wu-Shung used honeycomb core with a smaller cell size than considered as part of this experimental study. In addition, Wu and Wu-Shung used test pieces where the broken edge cells were trimmed. Both these factors may possibly reduce irregular folding of the edge columns thereby reducing ‘edge effect’, although verification would require additional experiments.

It has been found in previous research that under dynamic loading, crush strength values increase nonlinearly with impact velocity – numbers as much as 30% higher have been reported (Hexcel Composites). For the experiments reported here there was a linear relationship observed between impact velocity – over the range of 4m/s to 15m/s – and measured crush strength for the three densities of aluminium honeycomb core tested (Figure 6 to Figure 8). The correlation coefficient ranged from 0.93 for the 3/8-3.7 to 0.97 for the 1/4-5.2 cores – values close to 1 indicate excellent linear relationship. These relationships appear to be a reasonably accurate indication of the aluminium honeycomb core behaviour for the range of impact velocities and for the impact scenario covered by the experiments. Based on these relationships, the crush strength at point of impact for a 56km/h vehicle impact test is likely to be between 20% (3/4-1.8 aluminium honeycomb core) and 40% (1/4-5.2 aluminium honeycomb core) higher than its quasi-static crush strength. It must also be noted that the gradient of the straight line defining the relationship is greater for the higher density honeycomb cores, possibly indicating the enhancement is mass dependent. Confirmation would require additional experimental testing with higher density core that is beyond the capability of the test equipment used in this study.

Dynamic Crush Strength - 3/4-1.8 Aluminium Honeycomb Core
(crush area 125mm x 125mm)

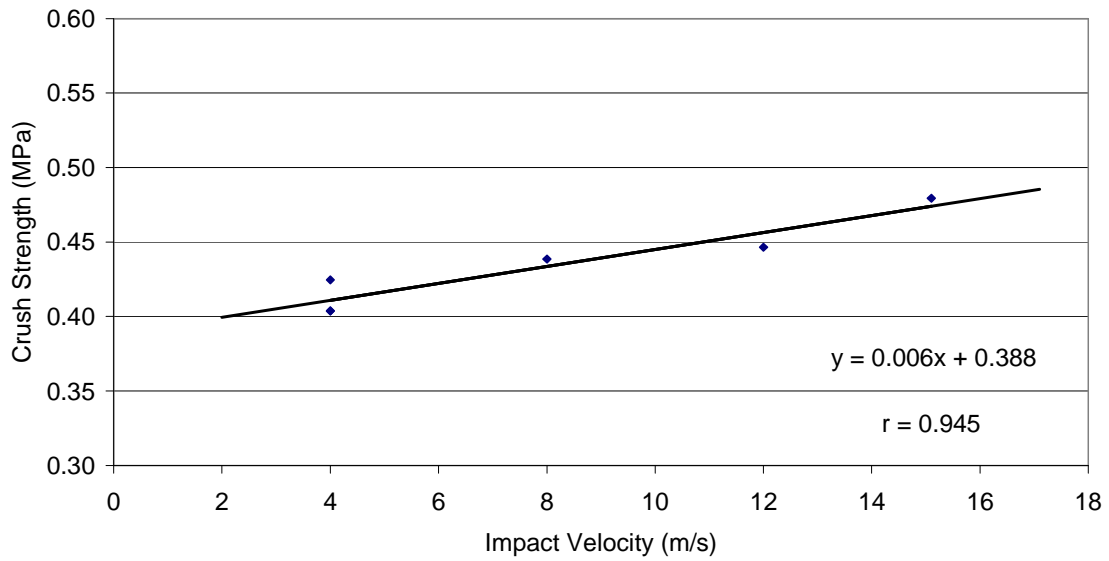


Figure 6: Change in dynamic crush strength with impact velocity for the 3/4-1.8 aluminium honeycomb core.

Dynamic Crush Strength - 3/8-3.7 Aluminium Honeycomb Core
(crush area 125mm x 125mm)

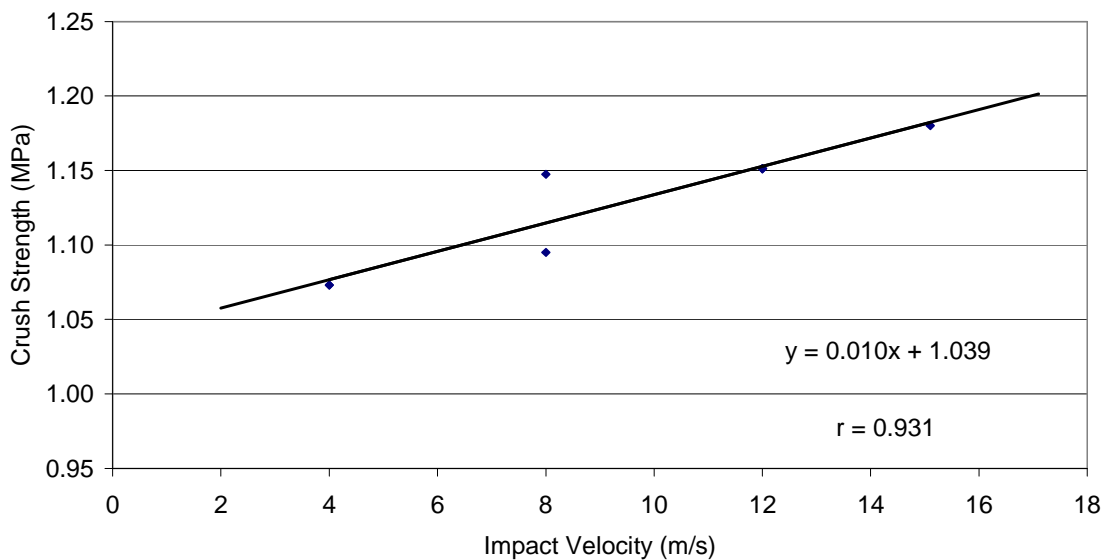


Figure 7: Change in dynamic crush strength with impact velocity for the 3/8-3.7 aluminium honeycomb core.

Dynamic Crush Strength - 1/4-5.2 Aluminium Honeycomb Core
(crush area 125mm x 125mm)

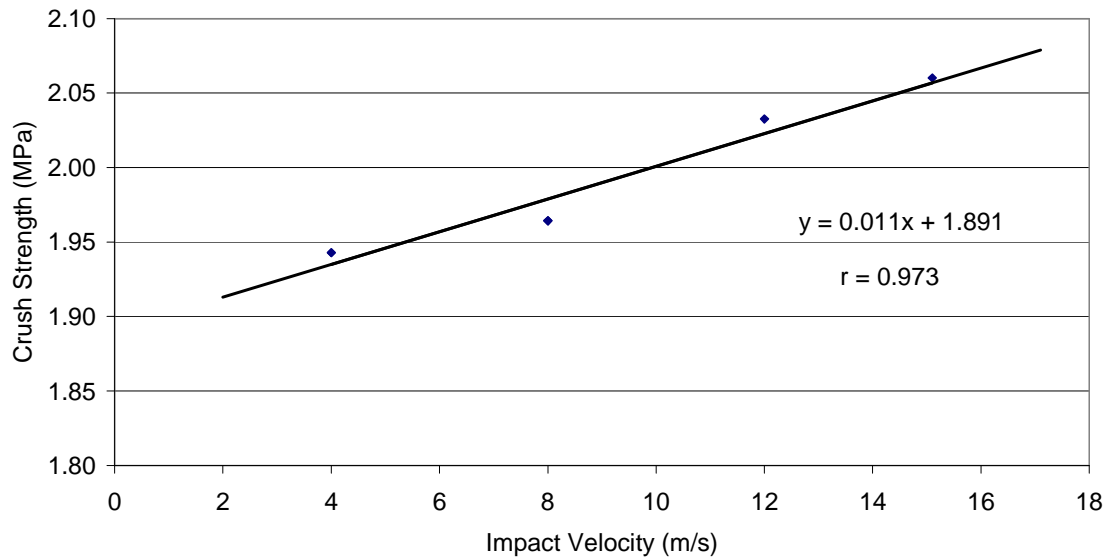


Figure 8: Change in dynamic crush strength with impact velocity for the 1/4-5.2 aluminium honeycomb core.

Studies by Wu and Wu-Shung (1996), and Zhao and Gary (1998), also showed enhancement in crush strength when subject to dynamic loading. Wu and Wu-Shung observed this enhancement to be dependent on initial impact velocity as for the present experimental study. However, Zhao and Gary observed no discernable change in enhancement with change in impact velocity (range 2m/s to 28m/s). This constant enhancement with increasing impact velocity may be considered unusual given the probable explanations for crush strength enhancement detailed later, and may be a consequence of the Split Hopkinson Pressure Bar arrangement used by Zhao and Gary.

A model by Wierzbicki (1983) predicted core crush strength to be dependent on material flow stress and the so-called relative cell thickness. The relative cell thickness is the cell wall thickness divided by the minor cell diameter (the shortest distance between two opposite sides of the hexagonal cell). The equation is:

$$p_m = 16.56\sigma_0 \left(\frac{h}{S}\right)^{5/3}$$

Where p_m , σ_0 , h and S are mean crushing pressure, flow stress of foils, cell wall thickness and minor cell diameter, respectively. Increases in the crush strength could then be attributed to a different flow stress under dynamic loading. However, both Wu and Wu-Shung (1996) and Zhao and Gary (1998) demonstrated that change in flow stress of the material when subject to dynamic impact would only account for part of the observed crush strength increase in the respective experimental studies. Other contributory factors considered were structural inertia – crush strength enhancement observed to increase with mass density – and a stabilisation effect due to lateral inertia. These inertial effects are believed to be the reason for columns displaying a more compacted plastic folding failure in dynamic loading, especially the edge columns (Figure 9). This more compacted folding of the edge columns would to some extent explain why static crush strength values predicted by extrapolating the dynamic relationships found in this study to the Y axis are higher than observed for quasi-static crush using similar sized blocks.



Quasi-static



Dynamic

Figure 9: Difference in deformation between quasi-static and dynamic loading conditions for 3/4-1.8 core showing more compacted plastic deformation of the edge columns for the dynamic loading condition.

Increasing the relative density of the honeycomb increases the relative thickness of the cell walls, meaning that the cell walls touch sooner, reducing the strain at which densification begins (Gibson and Ashby, 1998). Densification of the honeycomb core would limit effectiveness of as a barrier face as once the densification point is reached, further loading is resisted by force levels corresponding not to plastic buckling but to the core material as though solid. Based on the experimental results, the densification point for the three cores tested was derived for the higher energy impacts (Table 1) – the additional crush in these tests results in a more accurate determination of the densification point. It was observed that there was marginal difference in densification point for the two impact velocities, the higher density core having the slightly lower densification point.

Table 1: Derived values for densification point as a percentage of the initial core depth for the honeycomb cores tested as part of this experimental study.

Core	Velocity (m/s)	
	12	15
3/4-1.8	85%	85%
3/8-3.7	84%	83%
1/4-5.2	82%	81%

Previous research looking at aluminium honeycomb as an energy absorber stated that pre-crushing removed an elastic compressive peak. This was consistent with observation when the material is loaded quasi-statically. However, for the dynamic impacts the elastic compressive peak, observed to be up to 35% greater than the crush stress during the plastic deformation, was not removed. Pre-crushing of the aluminium honeycomb reduced this difference to less than 25%. It is considered that this is due to the inertia of the aluminium honeycomb material.

3.1.2 Penetration – Fixed load area

For the fixed area penetration tests, deformation of the honeycomb core was in axial crush ahead of the applied load and by tearing of the aluminium foil around the edge of the penetration (Figure 10). This response was observed to be the same irrespective of load condition – either quasi-static or dynamic. It must be noted that tearing was observed to initiate at the bond interface between neighbouring columns as opposed to the immediate edge of the load area. This would indicate that the

sharp edge of the penetrating object used in these tests was not a critical factor in determining honeycomb core response. Studies by Goldsmith et al (1992; 1995) have reported similar deformation response for penetration tests using a blunt cylinder as the penetrating object.

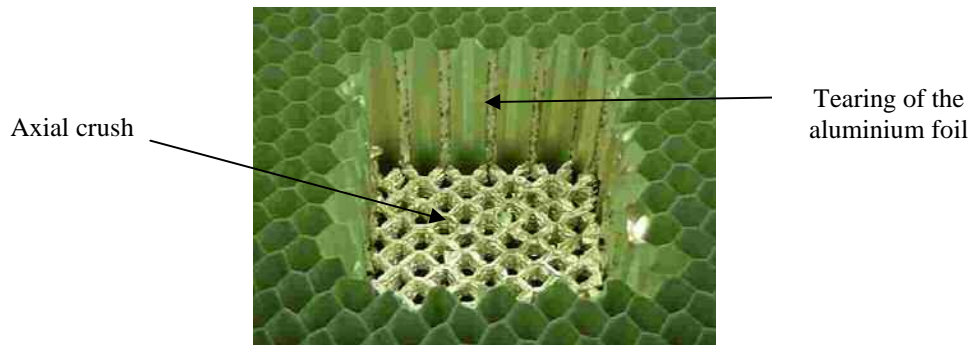


Figure 10: Post test view of the 3/4-1.8 aluminium honeycomb core showing the failure in axial crush and the tearing of the aluminium foil.

Estimation was made of the force required to tear the aluminium foil around the edge of the load area based on difference in measured load and that required for axial crush of the core ahead of the applied load (Table 2). The ‘tear force’ increases with relative density due to the requirement to tear increased numbers of cell walls. It is also likely that density change due to variation in foil thickness would result in similar change in ‘tear force’, although this was not investigated. It should be noted that ‘tear force’ contribution as a proportion of measured load is dependent on the isoperimetric quotient. This is the relationship between the load area and the perimeter of the load area; a value of one indicates the lowest tear force contribution as a proportion of the measured force, a value closer to zero a higher tear force contribution.

Table 2: Estimate of the tear strength of the aluminium honeycomb foil based on penetration test results.

Core	Approximate Tear Strength (kN/m)
3/4 - 1.8	0.9
3/8 - 3.7	2.0
1/4 - 5.2	4.8

A previous internal TRL study estimated a comparable tear force contribution for the 3/4-1.8 core of 1.1kN/m. Although Goldsmith and Sackman (1992) mentioned that tearing of the foil around the edge of the penetration absorbed additional energy (15-18%) for similar displacement and hence would generate additional load (Energy = Force x Displacement). However, they did not estimate the additional load.

The higher density core was observed to result in greater load spread due to its higher shear strength – the core depth determining the actual load spread for a particular core type. Load spread for the purpose of this study was defined as the proportion of the measured load recorded by load cells not directly aligned with the applied load. The closer neighbouring cells to the load area the greater the proportion of load measured by those load cells. For load applied above the centre load cell of the 9x9 matrix, the proportion of load recorded by the load cells not directly in line with the applied load was as high as 20% in these experimental tests (honeycomb depth 375mm).

It was found that pre-crushing of the aluminium honeycomb spread the applied load over the less stiff uncrushed layer. This increased the load recorded by the load cell wall prior to penetration and

resulted in crush of the aluminium honeycomb around the edges of the applied load. For the 1/4-5.2 core, 20mm of pre-crush resulted in a peak load approximately twice that based on crush of the aluminium honeycomb core ahead of the applied load and that required to tear the foil around the edges of the applied load area. This crushing of the aluminium honeycomb around the edges of the applied load area eventually resulted in the failure of the pre-crushed layer in bending and penetration of the aluminium honeycomb (Figure 11). The experimental test results indicated that participation of the core outside the region of contact in the deformation process was dependent on the interrelation between the density of the core and the depth of the pre-crush. A thin layer of pre-crush (between 1 and 2mm) allowed for penetration to occur without much engagement of the neighbouring uncrushed core. This minimised changes in measured load and load distribution but had the benefit of reducing the elastic compressive peak. It could be commented that the effect of the pre-crushed layer was similar to that when using an aluminium plate in front of the honeycomb core to create a sandwich type structure (Goldsmith and Sackman, 1992).

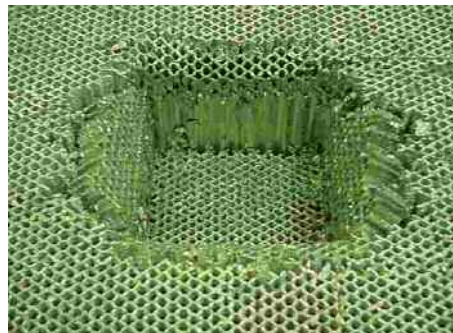


Figure 11: Resultant partial crushing of the region of uncrushed core adjacent to the area of the applied load prior to the failure of the pre-crushed layer in bending.

3.1.3 Penetration – Increasing load area

Failure of the honeycomb core in these experiments was observed to be a combination of out-of-plane crush (T direction), in-plane crush (L or W direction) and tearing (LT or WT plane). This was similar to the deformation mode observed in previous experimental study by Goldsmith and Louie (1995) when using a profiled projectile (sphere) to penetrate aluminium honeycomb core.

For the quasi-static loading condition the measured load increased linearly with penetration depth. This result was as expected since the load area increased linearly with penetration depth. However, load distribution altered from an initial alignment with the penetration centre line to the outer edges of the load cell wall. This was due to rotation of the honeycomb core either side of the penetration resulting in the outside edges of the rear face being heavily loaded (Figure 12). At a certain penetration depth the block would fracture along the penetration centreline due to the tensile stress in the L or W direction exceeding the fracture stress of the material.

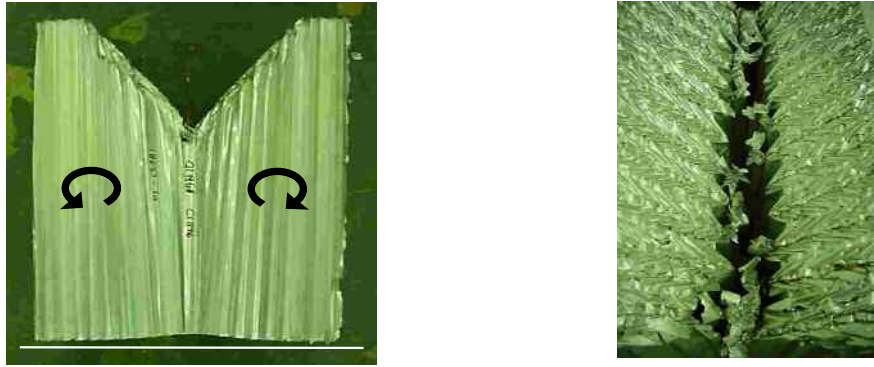


Figure 12: Deformation of aluminium honeycomb block. Note the rotation, the alignment of the rear surface with the horizontal and resultant fracture.

Rotation of the core either side of the penetration would be dependent on the moment arm (the distance of the applied load from the point of rotation) and the second moment of area (the distribution of mass about the point of rotation). Additional tests with the penetration offset from the centre of the block resulted in greater rotation of the ‘smaller’ and less rotation of the ‘larger’ portion of the block respectively – the rotation of the smaller portion of the block resulted in localised buckling of the cells at the outer edge. The rotation of the block either side of the penetration was accommodated for by elongation in the direction of the in-plane loading and narrowing perpendicular to the in-plane loading. The negative ratio of the strains perpendicular to, and parallel to, the in-plane loading define the Poisson Ratio of the aluminium honeycomb (Gibson and Ashby, 1988).

For the dynamic load condition, the majority of the load applied by the honeycomb core rear face was to those load cells directly in line with the leading edge of the wedge, the overall load being far higher than observed for the quasi-static load condition. This was most likely due to the inertia considerations detailed previously in the uniform crush tests. Up to a point, this would prevent rotation and the splitting of the block observed in the quasi-static crush tests.

4 Mathematical Modelling

This investigation assessed the ability of numerical modelling of aluminium honeycomb to predict the force transmission (load level and distribution) observed in the experimental study.

4.1 Preliminary Assessment

Two different approaches to modelling aluminium honeycomb were considered; a discrete mesh and a continuous mesh. An assessment of each approach was based on a prediction of the load cell wall measured load and the load distribution resulting from quasi-static uniform crush and fixed load area (penetration) simulations of a 375mm x 375mm honeycomb block fronting a 3 x 3 load cell wall matrix. The load cell spacing was 125mm x 125mm – the same as that used in the experimental tests and proposed for use in the assessment of vehicle crashworthiness. To take account of plastic deformations, both these modelling schemes are programmed as non-linear systems.

4.1.1 Continuous mesh model

The continuous mesh model is formed of individual columns of honeycomb elements joined together at common nodes. This forms a continuous mesh in all three core directions (expansion, ribbon and primary). The continuous mesh model used in this assessment takes material properties and mesh density characteristics from a model of the ECE R94 offset deformable barrier face developed in the mathematical modelling package RADIOSS (Mecalog Group). The mesh density was kept the same

as the source model as the source model is considered to represent a good balance between accuracy and run time for a car-to-barrier impact simulation.

For the uniform crush simulations, the predicted load was determined by the honeycomb element crush stress. For the continuous mesh model this corresponded to the quasi-static crush stress of the simulated aluminium honeycomb. For dynamic impact simulation the crush stress of the honeycomb elements would have to be adjusted to account for the enhancement in the crush stress observed in the experimental study. Changes to the honeycomb element crush stress would need to be validated using experimental data. In addition, the densification point of the honeycomb elements in the continuous mesh model was at 50% volumetric strain whereas for the actual aluminium honeycomb the densification point was observed to occur at 80% volumetric strain. For accurate prediction of the measured load at higher volumetric strains the densification point of the honeycomb elements would need to be adjusted to correspond with that of the simulated aluminium honeycomb.

For the uniform crush simulations the load distribution predicted by the load cell wall was determinate on the node distribution cross the rear face of the honeycomb model. The nodes act as focal points for load transfer between the honeycomb model and the load cell wall. For the continuous mesh honeycomb model, the coarse mesh density resulted in misappropriation of the applied load between the load cells, each node being representative of a load area not necessarily aligned with a single load cell. Due to the sharing of nodes in the continuous mesh model, it would not always be possible to align the nodes in such a way that each node and its associated load area align with a single load cell. Increasing the mesh density is the most appropriate approach to minimising misappropriation of the applied load in these circumstances. However, the mesh density was not increased at this stage due to the requirement to maintain an appropriate balance between run time/cost and accuracy.

For the fixed load area simulations, the continuous mesh prevented localised penetration and resulted in significant deformation of surrounding honeycomb material (Figure 13). This resulted in the predicted load at the load cell wall being greater than observed during the physical experiments due to the additional effort required to deform the surrounding honeycomb material. Predicted load spread was also greater than observed in the experimental tests. In addition, rotation of the projectile applying the load was noted in a number of the simulations (Figure 14). This rotation was attributed to the low mesh density resulting in only a few nodes being in alignment with the projectile and hence the potential for an increased moment arm – the distance between the resolved centre of the resisting force and the centre of gravity of the projectile. Note that the projectile in these simulations was in free flight.

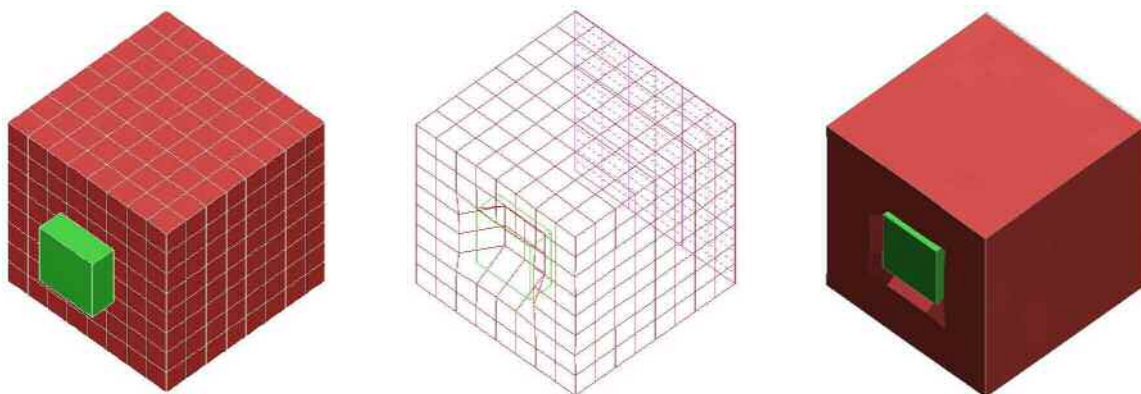


Figure 13: Central penetration simulation showing the additional deformation of the honeycomb material surrounding the projectile.

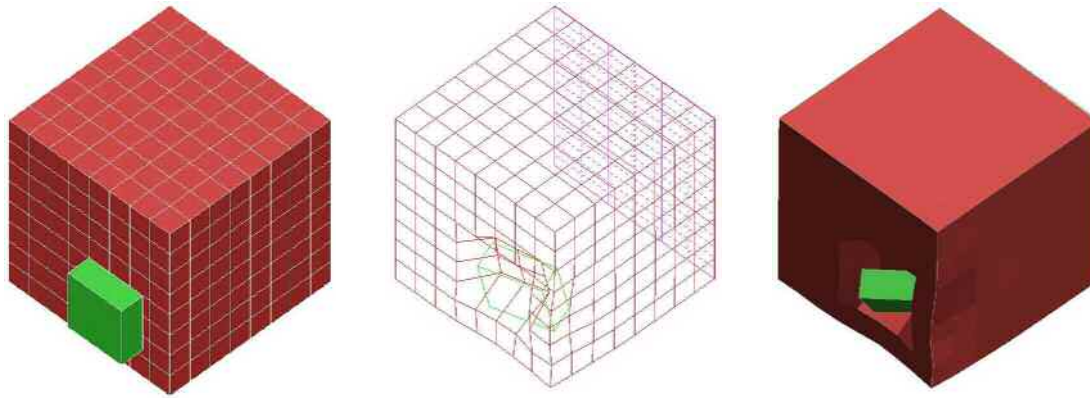


Figure 14: Offset penetration simulation showing both the additional deformation of the honeycomb material surrounding the projectile and the rotation of the projectile.

4.1.2 Discrete mesh model

The discrete mesh model is made up from separate columns of honeycomb elements aligned in the primary direction of the honeycomb between which there are beam elements with predetermined failure load to simulate a shear response consistent with aluminium honeycomb (Figure 15). The discrete mesh model used in this assessment was extracted from a model of the ECE R94 offset impact barrier face developed by Ove Arup and Partners International. Minimal scaling of the column spacing in the ribbon and expansion directions to match the 375mm x 375mm load cell wall frontal area resulted in a 7 x 8 column model (the column spacing varied in the ribbon and expansion directions in the source model). The mesh density was kept the same as the source model as this was considered to represent the best balance between accuracy and run time for a car-to-barrier impact simulation. Further details of how the offset barrier model was generated and validated are contained in the document ‘EEVC Offset Deformable Barrier LS-DYNA Model – Revision 2’ (Ove-Arup and Partners International).

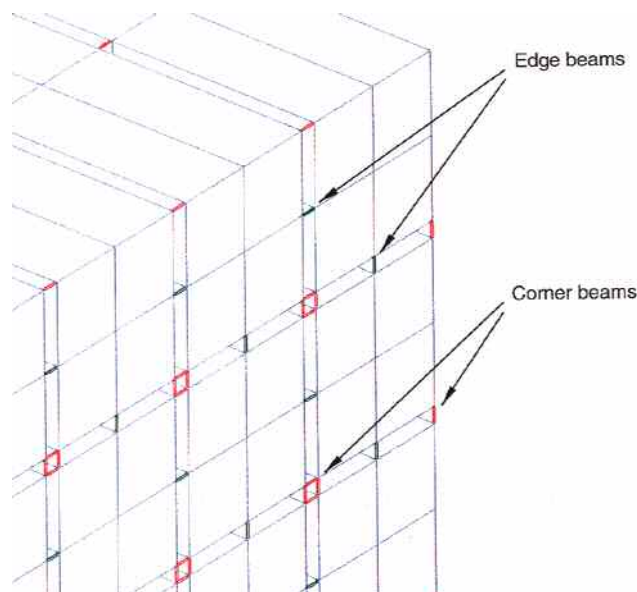


Figure 15: Close-up of the discrete mesh honeycomb model showing the beams that connect the honeycomb columns (gaps magnified).

For the uniform crush simulations, the predicted load at the load cell wall was observed to increase with crush depth. This was due to the crush stress of the honeycomb material used in the model increasing gradually with higher volumetric strains until a densification point at 80% volumetric strain. A consequence of the increase in crush stress with volumetric strain was that crush was shared between the elements through the depth of the block. A change in block height would alter the volumetric strain of the individual elements for a given block crush depth and hence alter the rate of increase in the load cell wall measured load. As for the continuous mesh model, the alignment of the nodes with the load cell wall resulted in misappropriation of the applied load. However, unlike the continuous mesh approach, generating a uniform load distribution when subject to uniform crush would only require that each column within the block is aligned with a single load cell. This is due to the fact that unlike the continuous mesh model there are no shared nodes between individual columns - the nodes for each column representing only the load applied by that column in isolation.

For the fixed load area simulations, failure of the connecting beams between those columns under axial load and those subject to shear loading allowed for localised penetration consistent with observation from the experimental study (Figure 16). The failure of the connecting beams along the edge of the load area contributed to an increase in the predicted measured load akin to that in the experimental study due to tearing of the aluminium foil around the penetration perimeter. However, there was failure of the connecting beams at each level within the model prior to densification of the honeycomb elements at that level. This was a consequence of the gradual increase in the honeycomb element crush stress with increase in volumetric strain; as the crush stress increased the following layer of elements would deform in preference resulting in failure of the connecting beams at that level (beam failure determined by an 'extension-based' criterion). The result would be differences in measured load and load distribution with greater crush depths. In addition, for the actual honeycomb tearing of the aluminium foil can occur at each cell join. This would require that column spacing within the model is matched to cell spacing of the actual aluminium honeycomb.

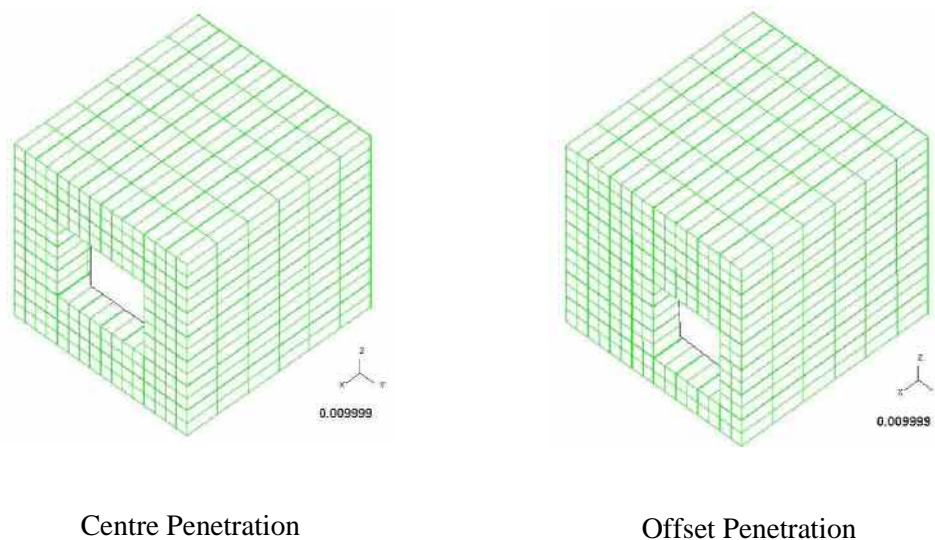


Figure 16: Penetration simulations showing failure of connecting beams minimising deformation of the honeycomb core material around the projectile.

4.1.3 Model comparison

Crush stress of the continuous mesh model was constant with increasing volumetric strain resulting in crush concentration of the block face consistent with experimental tests. However, the gradual increase in crush stress with increasing volumetric strains for the discrete mesh model resulted in crush distribution through the depth of the block. It is likely that the crush distribution observed in the

discrete mesh model would lead to inertial effects when the model is loaded dynamically – as impact speed increases the amount of crush at each layer prior to failure of the following layer would also increase.

Densification point for the continuous and discrete mesh models was at 50% and 80% volumetric strain respectively. In comparison, densification point for the aluminium honeycomb was at 80% to 85% of the uncrushed depth.

There was no provision in either honeycomb model for simulating the dynamic enhancement with increasing crush velocity noted in the experimental tests. This would require that the crush stress defined for the honeycomb elements is matched to the initial impact conditions, which would require validation data to accompany any changes.

Measured load distribution when subject to uniform crush was dependent on the node distribution across the rear face of the block for both approaches. This was due to the fact that load transfer between the honeycomb block and the load cell wall occurs through nodes, each representative of an area of the rear face of the block that may not necessarily be aligned with a single load cell. For both the continuous and discrete mesh model, increasing the mesh density would minimise misappropriation of the applied load. However, for the discrete mesh model, uniform load distribution could also be achieved by ensuring that each column is aligned with a single load cell – there being no shared nodes between the individual columns unlike the continuous mesh model. Within reason this would allow for the mesh density to be chosen based on other considerations.

Fixed area loading of the continuous mesh model resulted in significant distortion of the surrounding honeycomb material. The use of beam elements with a predetermined failure load connecting the columns in the discrete mesh allowed for penetration of the aluminium honeycomb to be modelled without large distortions of the surrounding material, which was consistent with experimental tests. However, the failure of the connecting beam elements through the depth of the block prior to the densification point being reached would result in errors in the measured load and load distribution for greater crush depths.

Based on the above, it was concluded that the discrete mesh model offered the greater potential for generating accurate load cell wall measured load and load distribution. This was due to the model's ability to distribute load correctly across the load cell wall without necessarily increasing mesh density and to model localised penetration consistent with that observed in the experimental study. A more detailed assessment of the discrete mesh approach for predicting load cell wall measured load and load distribution was therefore undertaken. For accurate prediction the column spacing would need to match the honeycomb cell spacing.

4.2 Discrete Mesh Honeycomb Assessment

This section describes a detailed assessment of the discrete mesh approach to modelling aluminium honeycomb. The basis for this assessment was the discrete mesh model of the EEVC offset barrier face developed by Ove Arup and Consultants. Consideration was given to differences between the honeycomb models that had been used in the barrier face model and the properties of the actual aluminium honeycombs. This allowed sections of the barrier model to be simplified to represent a single honeycomb block. Following this a process of model alteration and impact simulation was undertaken with the aim of generating load cell wall measured load and load distributions consistent with the experimental tests.

4.2.1 Model characteristics

The ECE R94 offset deformable barrier face model consists of a 3/4-1.8 honeycomb main block fronted by 1/4-5.2 honeycomb bumper elements (Figure 17). As part of the assessment of the discrete mesh approach to modelling aluminium honeycomb consideration was given to possible parameter tuning that may have been made to the 3/4-1.8 and 1/4-5.2 honeycomb models as part of the validation of the offset deformable barrier face model. Recommendations were then made regarding

alterations to the 3/4-1.8 and 1/4-5.2 honeycomb models for this study and for areas requiring further investigation.

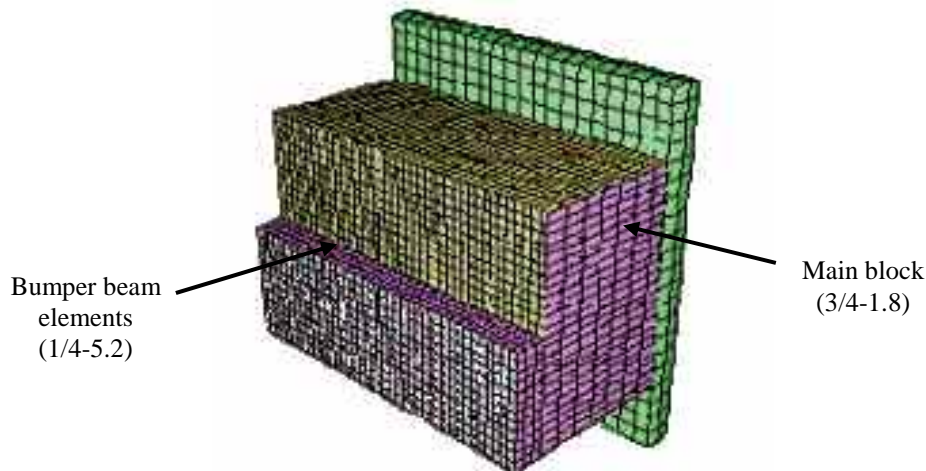


Figure 17: EEVC 40% offset deformable barrier impact model developed by Ove Arup consultants.

The discrete mesh approach to modelling aluminium honeycomb connects columns of honeycomb elements aligned in the primary core direction by beam elements with a predetermined failure load in the ribbon and expansion directions. Two types of beam elements are used in connecting the columns, corner and edge beams (Figure 15). The failure load of an edge beam is set at double that of a corner beam, because in any given direction the corner beams exist in pairs and the edge beams singly. Failure of the beams occurs based on an extension based criterion. This means that the stiffness of the beams is very high until a yield force is reached. As the loading continues to increase, the yield force is reduced linearly with plastic extension, reaching zero at 0.5mm extension. When the beam exceeds this extension, it fails and is unable to carry any load.

For the 3/4-1.8 honeycomb model the yield forces of the connecting beams were set at 120N and 240N for the corner and edge beams respectively, whilst for the 1/4-5.2 honeycomb model they were set at 800N and 1600N. Based on an approximate column spacing of 50mm as found in the offset deformable barrier face model these values equate to failure loads per unit length in the expansion and ribbon direction of 9.6kN/m and 64kN/m for the 3/4-1.8 and 1/4-5.2 honeycomb models respectively. However, these values are not necessarily directly comparable to the tear force measured in the experimental tests due to effect of beam spacing in the primary direction and the pattern of beam loading in the primary direction.

The 3/4-1.8 honeycomb was modelled as discrete in both ribbon and expansion directions with only slight variation in column spacing to match the barrier face external dimensions (Figure 18). However, the 1/4-5.2 honeycomb was modelled as discrete in the expansion direction, with the same column spacing as for the 3/4-1.8 honeycomb model, but continuous in the ribbon direction (Figure 18). This was due to the division of the 1/4-5.2 honeycomb into three bumper beam elements in the ribbon direction which, combined with the sandwiching of these bumper beam elements between aluminium facing plates, meant shear failure in that direction was unlikely. In the expansion direction of the 1/4-5.2 honeycomb model the connecting beams along the front and rear face were prevented from failure in order to simulate the higher shear strength of the aluminium facing plates in comparison to the aluminium honeycomb behind.

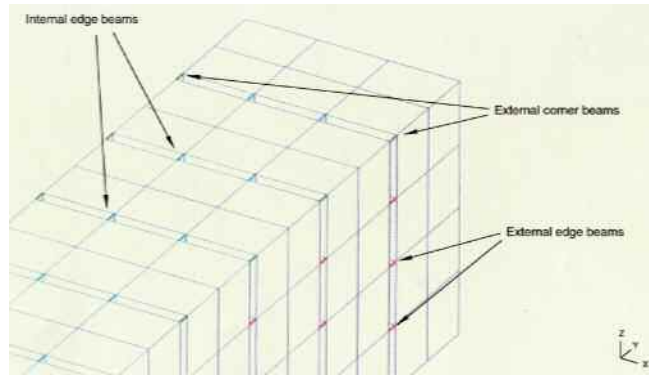


Figure 18: Close up of the 1/4-5.2 honeycomb model used to simulate the bumper beams of the offset frontal impact barrier.

The mass densities of the 3/4-1.8 and 1/4-5.2 honeycomb models were set at 83kg/m³. In comparison, the 3/4-1.8 and 1/4-5.2 aluminium honeycombs were 29kg/m³ and 82kg/m³ respectively. The higher mass density of the 3/4-1.8 honeycomb model leads to increased inertia when subject to dynamic loading – a potential issue when the crush is distributed between the honeycomb elements along the column depth. In addition, it was noted that the mass density of the honeycomb model under evaluation was not only dependent on the mass of the honeycomb material model elements, but also the mass of the shell elements used to define the contact surfaces between the individual honeycomb columns. The shell elements contributed to a significant proportion of the final overall mass of the barrier model. Any changes in the mesh density, and hence the total column surface area, would have an effect on the mass density of the given honeycomb model and hence the response to dynamic loading.

The axial crush stresses of the honeycomb models are approximately 30% higher than the quasi-static crush stresses of the corresponding aluminium honeycombs (Figure 19 and Figure 20). This is a reflection of the larger crush stresses experienced in dynamic impacts – the offset barrier face model from which the honeycomb models were extracted is used to simulate a 15.6m/s impact. The honeycomb material model itself has no provision for simulating the dynamic enhancement with increasing crush velocity, requiring that crush stress is matched to initial impact conditions. Axial crush stresses in the ribbon and expansion directions of the core models were the same and were 10% of the axial crush stress in the primary direction. In comparison, axial crush stress in ribbon and expansion directions of the aluminium honeycomb vary slightly due to the core being non-isotropic, and were lower than for the honeycomb model, typically less than 5% of the axial crush stress in the primary direction.

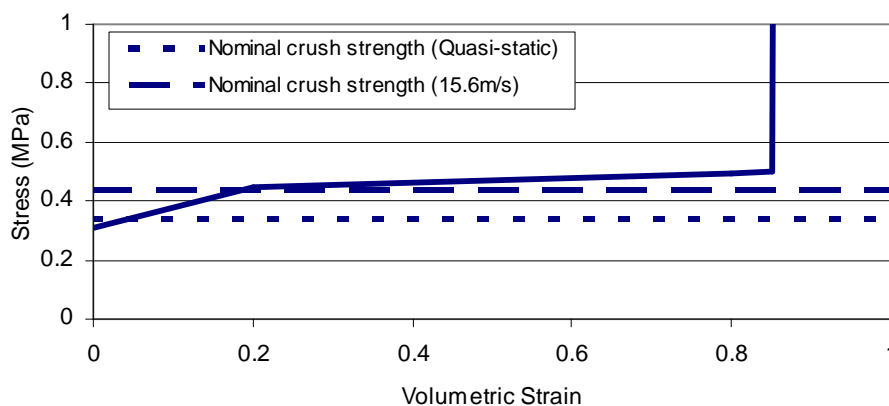


Figure 19: Crush stress against volumetric strain for the 3/4-1.8 honeycomb model in the primary (X) direction (solid line). The quasi-static and dynamic crush strength for the actual aluminium honeycomb are shown for reference (dashed lines).

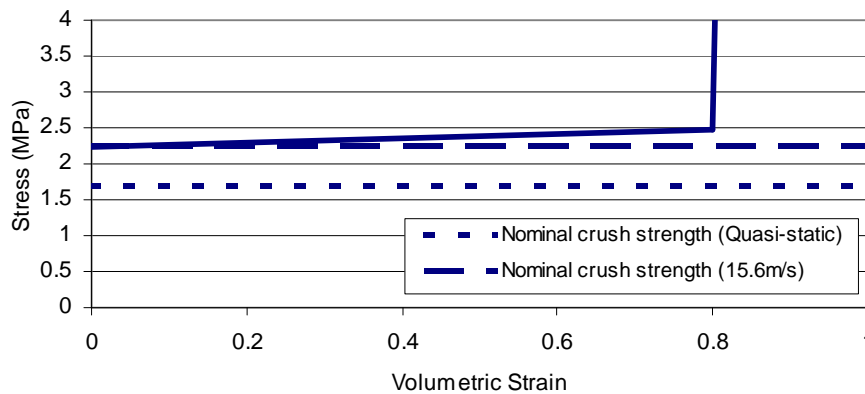


Figure 20: Crush stress against volumetric strain for the 1/4-5.2 honeycomb model in the primary (X) direction (solid line). The quasi-static and dynamic crush strength for the actual aluminium honeycomb are shown for reference (dashed lines).

Shear stress was the same in both the ribbon and expansion directions of the honeycomb model. The shear stress values varied from 0.224MPa at 20% volumetric strain to 0.247MPa at 80% volumetric strain for the 3/4-1.8 honeycomb model and 1.12MPa at 0% volumetric strain to 1.23MPa at 80% volumetric strain for the 1/4-5.2 honeycomb model. At 80% volumetric strain the honeycomb becomes compacted. In comparison for the aluminium honeycomb the shear stress varies with orientation. The actual values are 0.41MPa and 0.69MPa for the 3/4-1.8 aluminium honeycomb and 1.49MPa and 2.49MPa for the 1/4-5.2 aluminium honeycomb.

The following comments can be made regarding adaptation of the honeycomb models used in the offset deformable barrier face model to predict force transmission observed in the experimental study:

Beam Failure Load: Until the effect of beam spacing and the pattern of beam loading in the primary core direction can be established, the failure load of the connecting beams should be adjusted with changes in mesh density so as to maintain a consistent failure load per unit length.

Model Construction: In the offset deformable barrier face model the 1/4-5.2 honeycomb was modelled as continuous in one direction and failure of the beam elements along the front and rear faces were prevented. For the purposes of this study the 1/4-5.2 core was modelled as discrete in both the ribbon and expansion directions and the provision for preventing failure of the beams elements along the front and rear face was removed.

Mass Density: The mass of the barrier face model was a combination of the shell elements that define contact between the columns and the honeycomb material. In the case of the 3/4-1.8 honeycomb model – the main block of the barrier face model – the mass density was higher than that of the actual aluminium honeycomb. For the 1/4-5.2 honeycomb model – the bumper beam elements – the mass density was similar to that of the actual aluminium honeycomb. For the purpose of the study, the mass of the shell elements was set to zero mass to remove a mass density dependency on mesh density and the mass density of the honeycomb models was matched to that of the actual aluminium honeycomb.

Honeycomb Material Crush Stress: There was no provision for simulating the dynamic enhancement with increasing crush velocity noted in the experimental tests. The crush stresses of the 3/4-1.8 and 1/4-5.2 honeycomb models corresponded to the dynamic crush stress when impacted at 15.6m/s (the offset deformable barrier test speed). For the purpose of the study, the crush stress of the honeycomb models was matched with the quasi-static crush stress of the aluminium honeycomb. This would allow for comparison with the experimental quasi-static crush test results.

Shear Stress: The lower shear stiffness of the honeycomb model would result in less load spread ahead of the applied load. This would only be an issue if the column cross-sectional area was significant in relation to the localised load area. In addition, if the load area edge is offset from the column edge the strain of the connecting beam elements would be due to shear loading of the column

elements. The effect of the difference in shear stiffness between the honeycomb models and the aluminium honeycomb will be investigated in the study.

Mesh Density: The honeycomb model column spacing is not consistent with the load cell spacing. This would result in variation in the measured load distribution when subject to uniform crush. The column (mesh) density of the honeycomb model was increased so that the load cell wall spacing was exactly divisible by the column spacing and that the division between the loadcells was aligned with the division between the columns. This would prevent misappropriation of the applied load between different load cells.

4.2.2 Model development

Three different iterations of the discrete mesh model approach were considered. The first of these was based on the premise of minimal alteration to the source model so as to provide a baseline against which to assess future alterations. The column spacing was suitably scaled to align with a 3 x 3 load cell wall matrix and to ensure identical column spacing in both ribbon and expansion directions. This resulted in an 8x8 column block as opposed to the previous 8 x 7 column block considered in the preliminary assessment. In addition, alteration was made to the 1/4-5.2 core model to allow for shear failure in both the ribbon and expansion direction, and to remove the provision preventing shear failure of the connecting beam elements along the front and rear faces.

The other two iterations were developments of the 8x8 column block based on recommendations made in the previous section. Column density was increased in both ribbon and expansion directions such that each column was within an individual load cell. This was undertaken in two stages, the first an increase to a 9x9 column block (the load cell centreline aligned with column centreline), the second to a 12x12 column block (the load cell centreline aligned with the division between neighbouring columns). In each case, the beam element failure load and the honeycomb model element depth in the primary core direction were altered to maintain a beam failure load per unit length equivalent to the 8x8 column model in the three core directions. This required a slight alteration in block height between the three model iterations. In addition, the crush stress of the 3/4-1.8 honeycomb model was altered to remove the initial sharp increase observed over the first 20% volumetric strain and to align better with the quasi-static crush stress of the aluminium honeycomb. Table 3 details the differences between the three iterations of the 3/4-1.8 core model.

Table 3: Comparison of the properties of the 8x8 column 3/4-1.8 core model and the development 9x9 and 12x12 column models.

Model Iteration	8 x 8 column	9 x 9 column	12 x 12 column
Block Frontal Area	375mm x 375mm	375mm x 375mm	375mm x 375mm
Stress/Strain (curve definition to 80% volumetric strain)	0% 0.3104MPa 20% 0.4485MPa 80% 0.4933MPa	0% 0.33MPa 80% 0.40MPa	0% 0.33MPa 80% 0.40MPa
Failure Load / metre (ribbon and expansion directions)	9.6kN/m	9.6kN/m	9.6kN/m
Beam Failure Load* (edge & corner beams)	240N & 120N	200N & 100N	150N & 75N
Element Depth** (primary core direction)	67mm	56mm	42mm
Block Height	400mm	392mm	420mm

*Altered to maintain same failure load per unit length in the ribbon and expansion directions

**Altered to maintain same failure load per unit length in the primary core direction

A number of simulations were conducted to assess the load cell wall response to quasi-static and impact loading using the three different core model iterations detailed above. The simulation matrix is detailed in Appendix C. The loading configurations considered were uniform crush, offset crush with a load area equivalent to 50% of the block frontal area and fixed area penetration with a load area equivalent to one load cell. In addition, a number of exploratory simulations using a wedge projectile were performed although these are not discussed. This was due to the complications with predicting accurate force transmission and distribution for the fixed load area simulations

4.2.3 Results and discussion

There was variation in the predicted load between load cells for the uniform crush simulations using the 8x8 column block. This was due to the inconsistency of the node distribution with respect to the load cells. Alignment of the load cell division with column division in the 9x9 and 12x12 column blocks resulted in zero variance in the predicted load between load cells with the exception of the quasi-static crush simulation of the 12x12 column block. For this simulation it was noted that variance in the predicted load between load cells increased with crush depth due to column instability (Figure 21).

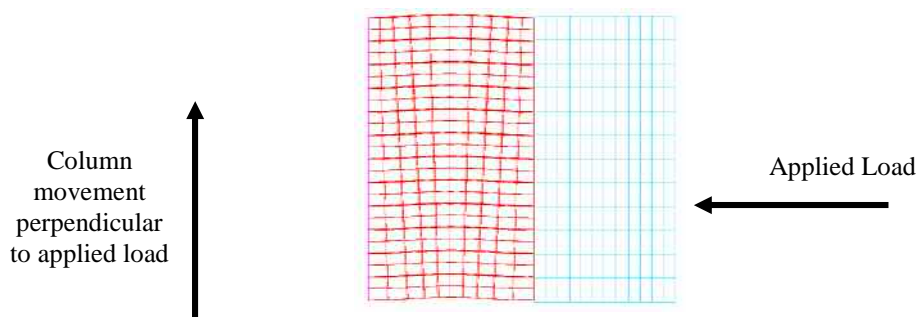


Figure 21: Quasi-static crush simulation of the 3/4-1.8 core 12x12 column block showing instability of the columns as the movement perpendicular to the direction of the applied load (the red part represents the honeycomb model, the light blue part the projectile applying the load).

Instability of the columns in the discrete mesh model approach was attributed to the connecting beam elements being allowed to rotate about their fixation. This allows for the relative movement of neighbouring columns and places greater emphasis on individual column stability in comparison to the continuous mesh approach in which the columns are stabilised by their neighbours. Column stability is dependent on loading condition, slenderness ratio (column area relative to height) and honeycomb element crush stress. These are detailed below – compared to the quasi-static crush of the 12x12 column model:

- Loading Condition: Changing from quasi-static to dynamic loading of the 12x12 column model removed column instability and resulted in zero variance in the measured load distribution. This was due to the inertia of the honeycomb model elements.
- Slenderness Ratio (Column Area): Increasing the column area by reducing the column density (12x12 to 9x9) resulted in zero variance in the measured load distribution.
- Slenderness Ratio (Column Height): The removal of one layer of honeycomb elements from the block to reduce individual column height resulted in zero variance in the measured load distribution.
- Crush Stress: Increasing the gradient of the stress-strain curve over the first 20% volumetric strain (source model stress-strain curve) was observed to reduce the column instability.

In the offset crush simulations the applied load has to overcome the crush stress of the elements and the connecting beams around the edge of the load area. The increase in crush stress of the honeycomb

elements and the subsequent failure of the connecting beams at each level can be observed in the ‘saw-tooth’ pattern of the load-displacement curve (Figure 22). The balance between the increase in element crush stress and the beam failure load determines the crush depth at which the beams fail at each level. For the simulation result shown, the beams throughout the depth of the block failed prior to the densification point of the honeycomb model. This would prevent prediction of measured load and load distributions at greater crush depths.

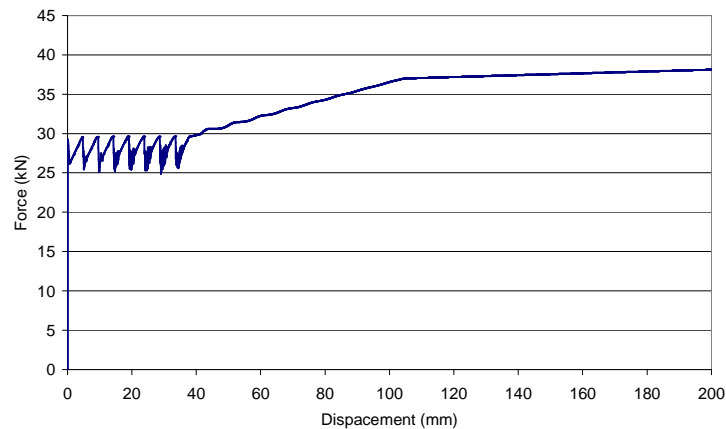


Figure 22: Measured load for the 50% offset crush simulation of the 3/4-1.8 core 8x8 column block showing variation over the first 40mm due to loading and subsequent failure of connecting beam elements at each level.

The effect of changing column alignment with the load area edge was assessed based on the offset crush simulations of the 9x9 and 12x12 columns blocks. For the 9x9 column block, the load area edge aligned with the centreline of one row of columns. This resulted in additional deformation of the honeycomb material between the load area edge and the column edge due to shear loading. In addition, strain of the connecting beam elements through shear loading of the column elements resulted in a different beam element response. Those beam elements along the front face of the block did not fail, resulting in shear strain of the front layer of column elements along the edge of the load area. In subsequent layers, only axial crush occurred. This difference in response was attributed to the front layer of beam elements only connecting to one layer of column elements, whilst those within the block are common to two layers of column elements and are therefore subject to higher shear loading.

In comparison, for the 12x12 column block the edge of the load area in the offset crush simulation aligned with the division between two rows of columns. The axial crush of the row aligned with the load area resulted in direct strain of the connecting beam elements between the columns. For the quasi-static simulation this resulted in shear strain of neighbouring column elements prior to beam element failure, whilst for the dynamic simulation inertial effects minimised shear strain of the neighbouring elements prior to beam element failure. Subsequent increase in crush depth resulted in loading and subsequent failure of the connecting beam elements at each level through the block with little additional shear strain of the neighbouring column elements.

The deformation of the 9x9 and 12x12 column blocks in the quasi-static offset crush simulations are shown in Figure 23. It was noted that in both the offset simulations using the 9x9 and the 12x12 column blocks that the additional load required to fail the connecting beam elements along one edge of the load area resulted in the greater concentration of the column element crush at the block face along that edge.

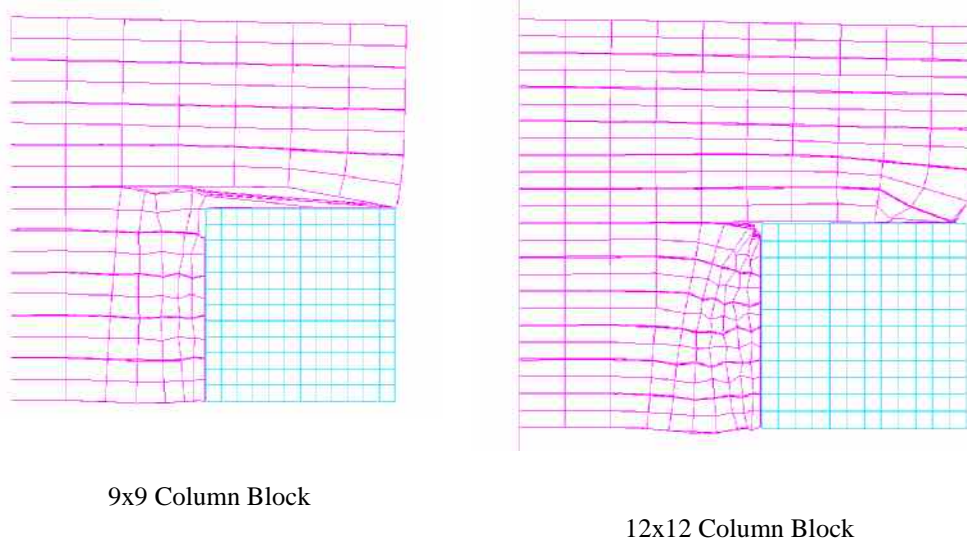


Figure 23: Difference in the deformation of the 3/4-1.8 core 12x12 and 9x9 column blocks in the quasi-static 50% offset crush simulations.

The change in crush stress between the 8x8 and the 9x9 and 12x12 column models resulted in greater crush of each layer of column elements prior to the failure of the supporting connecting beams. This can be viewed as the expanded ‘saw tooth’ pattern in the load against displacement trace when compared to that previously shown for the 8x8 column block (Figure 22 and Figure 24). The higher load for the 9x9 column block simulation was due to the crush of additional column elements along the edge of the load area, whilst the initial high load for the 12x12 column model over the first 80mm crush was due to the shear strain of the neighbouring column elements in the quasi-static crush simulation. Difference between the measured load and that based on axial crush of the material ahead of the load area is representative of the tear force contribution in the experimental tests. Estimates of tear force contribution in the offset simulation were 13kN/m for the 9x9 column block and 8kN/m for the 12x12 column block. Both these values were higher than those for the corresponding aluminium honeycomb.

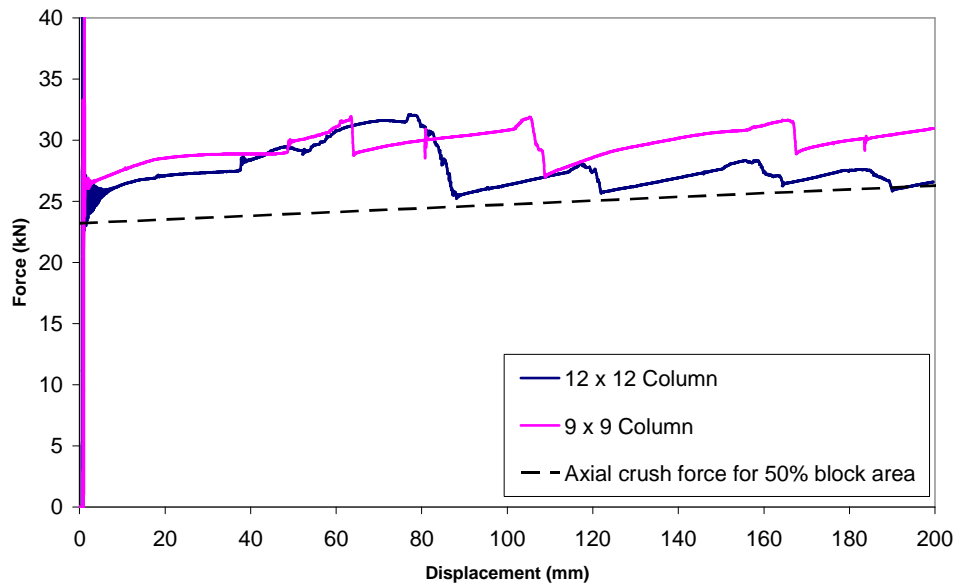


Figure 24: Predicted load at the load cell wall for the quasi-static offset crush simulations of the 3/4-1.8 core 9x9 and 12x12 column blocks in comparison to that required for axial crush of the honeycomb material ahead of the applied load.

Load distribution in the offset crush simulations was not consistent with the experimental tests. For the simulations, the highest loads were in general predicted by those load cells with only 50% overlap with the applied load. For the experimental observations, the highest loads were measured by those load cells with 100% overlap. In addition, the shear strain of the neighbouring elements when subject to quasi-static loading resulted in a significant proportion of the predicted load being recorded by those load cells not in alignment with the applied load area. These load cells would have been expected only to record a minimal proportion of the applied load. The load distribution for the quasi-static and dynamic offset loading simulations for the 3/4-1.8 core 12x12 column block are shown (Figure 25 and Figure 26).

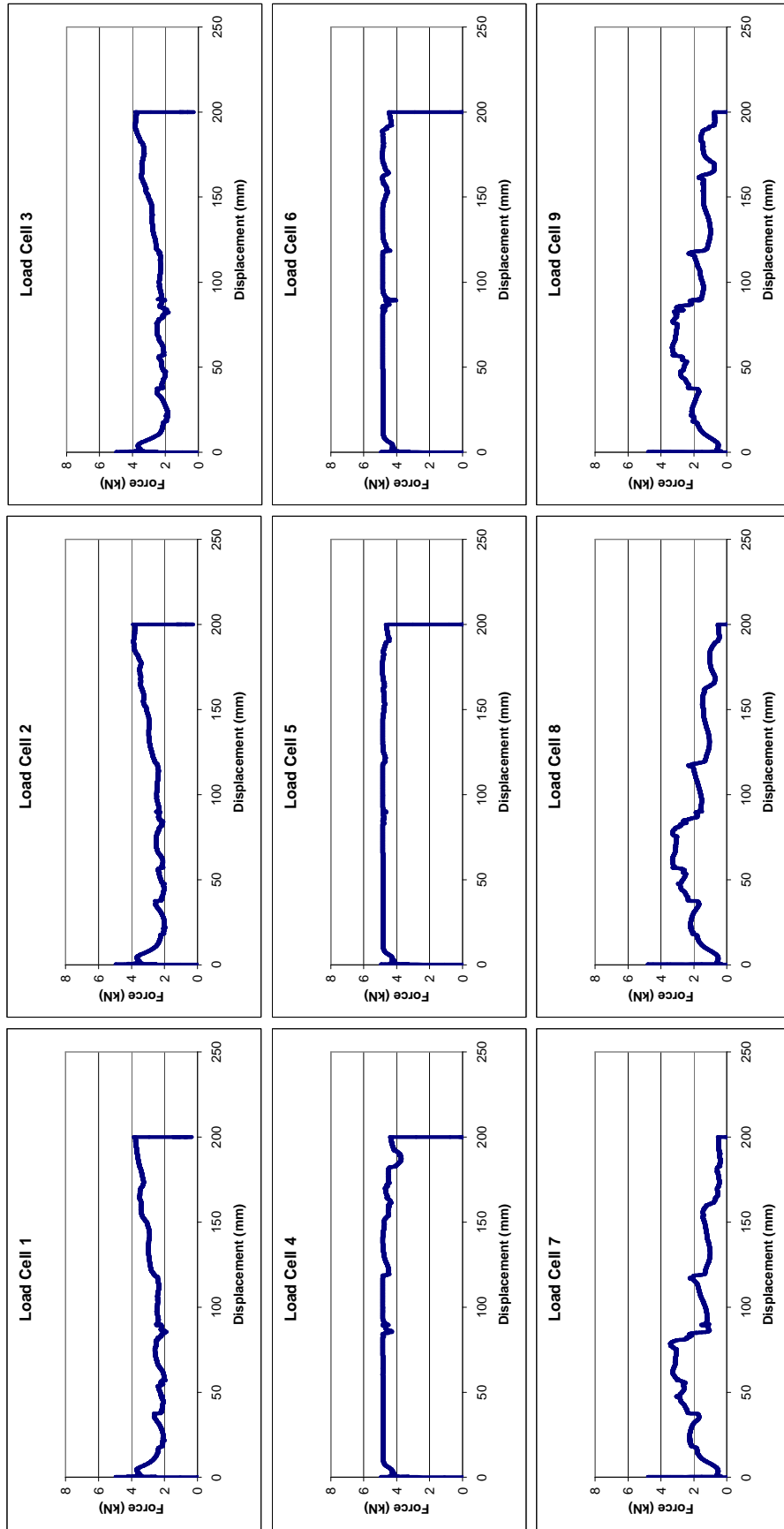


Figure 25: Load cell wall force distribution for quasi-static offset loading simulation for the 3/4-1.8 core 12 x 12 column block. The load area was aligned to engage 100% of load cells 1 to 3 and 50% of load cells 4 to 6.

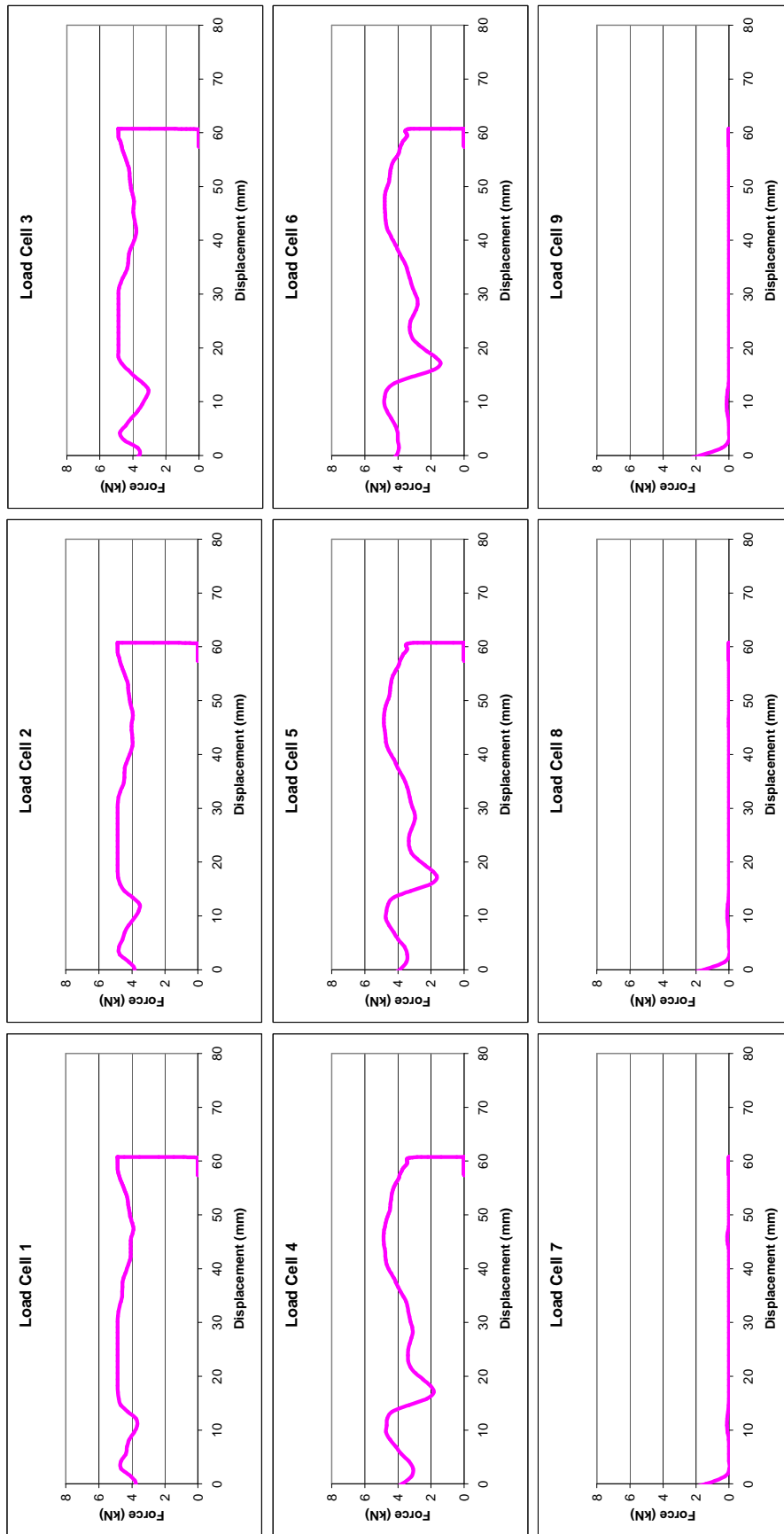


Figure 26: Load cell wall force distribution for 16m/s dynamic offset loading simulation for the 3/4-1.8 core 12 x 12 column block. The load area was aligned to engage 100% of load cells 1 to 3 and 50% of load cells 4 to 6.

To assess the effect of the connecting beam failure load and material crush stress upon measured load distribution a number of additional simulations using the 12x12 column model were performed. Beam failure load was adjusted in stages from 9.6kN/m down to 0kN/m. Reducing failure load of the beam elements resulted in lower overall load cell wall measured load and a load distribution more in line with expectation (Figure 27).

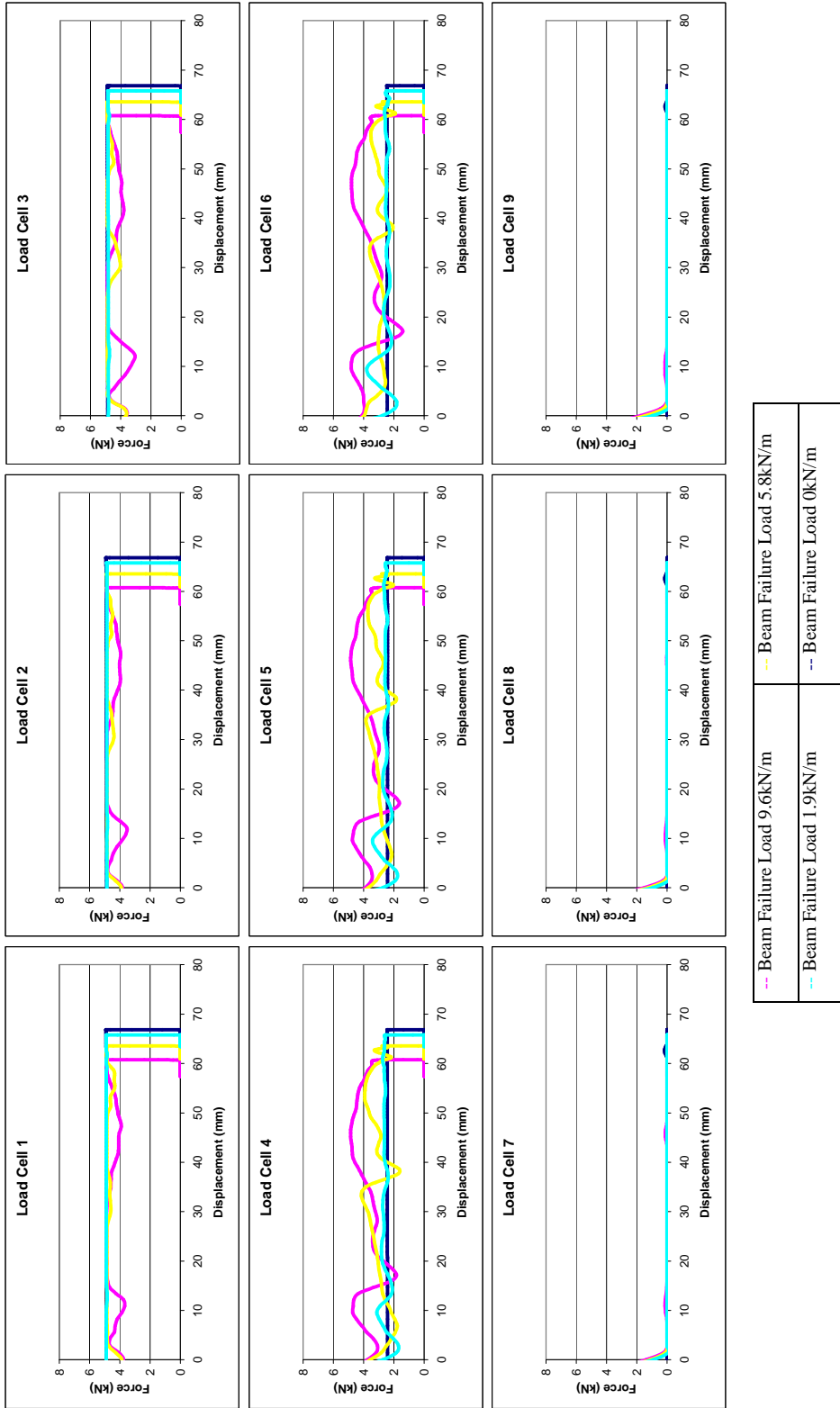


Figure 27: Measured load distributions for the 50% offset impact simulation of the 3/4-1.8 honeycomb core using different beam element properties.

Based on the results of the simulations, a relationship between the beam element failure strength and the additional load measured by the load cell wall in the offset loading simulations was derived (Table 4). The additional load can be taken to represent the tear strength of the aluminium honeycomb. Based on these results, the force per unit length required to fail the connecting beams should be set approximately 14%-18% higher than the tear strength of the simulated aluminium honeycomb.

Table 4: Different beam failure loads and the estimated tear force contribution based on offset simulations using the 3/4-1.8 core 12x12 column block.

Failure Load - based on beam strength (kN/m)	Additional Load - load cell wall results (kN/m)
9.6	8.3
5.8	5.1
1.9	1.6

For the material crush stress, additional simulations reverted to the source model properties. These were a high rate of increase in the crush stress for the initial 20% volumetric strain followed by a lower rate for the remainder of the volumetric strain until densification. The change in the crush strength characteristics of the honeycomb model resulted in a distinct oscillation in the load and the load distribution (Figure 28). The pattern of load redistribution as the beams at each level were loaded and failed was the same in both simulations, but the higher rate of increase in the element stiffness for the model using the source model crush strength properties meant that each layer of column elements deformed less prior to initiating failure of the weaker elements behind. This reduced the overall crush depth between successive layers of beam elements being loaded and failing, resulting in the oscillation in the measured load. As previously mentioned, failure of the connecting beams at each level prior to the densification point of the block being reached would cause a problem in generating accurate load cell wall measured load and load distribution at greater crush depths.

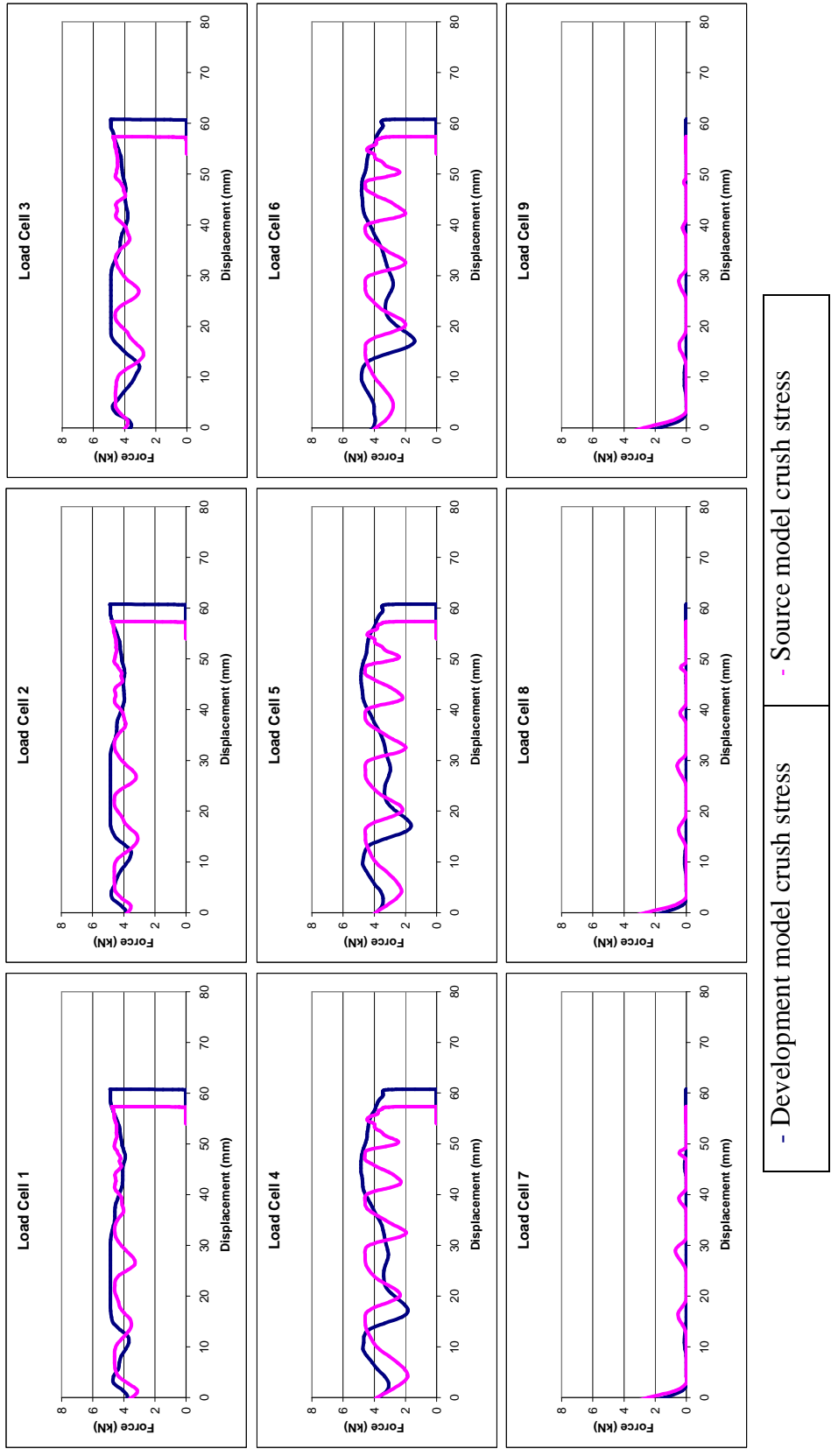


Figure 28: Comparison of the load cell wall force distributions for the 50% offset impact simulations using different stress/strain input curves.

5 Conclusions

5.1 Experimental Study

The experimental part of the study evaluated the force transmission characteristics of three types of aluminium honeycomb structure. The following can be concluded from this study:

When subjected to out-of-plane loading (load applied along the primary axis of the honeycomb):

- The crush stress of the aluminium honeycomb limited the load recorded by the load cell wall. The crush stress was shown to be dependent on the relative density, the velocity of the projectile and the proportion of columns unsupported along one edge. For the cores tested the relative density varied by a factor of three (3/4-1.8 to 1/4-5.2 core) resulting in a difference in crush stress of 1.4MPa (0.34MPa to 1.71MPa). For a vehicle impact velocity of 56km/h the result would be a 20-40% increase in crush stress (depending on relative density). A proportion of unsupported columns greater than 20% of the total resulted in a crush stress below the manufacturer quoted tolerance.
- Densification of the aluminium honeycomb resulted in further loading being resisted by force levels corresponding to the solid aluminium material. Increasing the relative density reduced the strain at which densification occurred. This densification point was related to the relative density of the aluminium honeycomb and ranged from 85% (3/4-1.8 core) to 81% (1/4-5.2 core) of the block depth. Densification point is expressed as a percentage of the uncrushed core depth.
- For dynamic loading, the initial elastic compressive peak was observed to be up to 35% greater than the crush stress during the plastic deformation stage. Pre-crushing of the aluminium honeycomb reduced this difference to less than 25%.

When subjected to localised penetration (out-of-plane loading):

- Localised penetration resulted in additional load being recorded by the load cell wall above that measured for axial crush. This was a result of the additional force required to tear the aluminium foil around the edge of penetration. This 'tear force' contribution was related to the relative density of the aluminium honeycomb and ranged from 0.9 kN/m (3/4-1.8 core) to 4.8 kN/m (1/4-5.2 core).
- Increasing the relative density and/or depth of the aluminium honeycomb core was observed to result in greater load spread. For the experimental tests, load spread through the aluminium honeycomb resulted in up to 20% of the applied load being recorded by load cells outside of the original load area.
- Pre-crushing of the aluminium honeycomb created a sandwich type structure, with the stiffer pre-crushed layer spreading the load over the less stiff uncrushed layer. For the 1/4-5.2 core, 20mm pre-crush approximately doubled the load recorded by the load cell wall prior to penetration. A thin (1-2mm) pre-crush was shown to reduce the initial compressive peak in the stress strain curve whilst not significantly increasing the measured load prior to penetration.

When subjected to localised (wedge) penetration resulting in both out-of-plane and in-plane loading:

- The addition of in-plane loading resulted in rotation of the aluminium honeycomb either side of the penetration centreline and/or fracture of the aluminium honeycomb block along the penetration centreline.
- Rotation of the aluminium honeycomb resulted in the redistribution of the load recorded by the load cell wall to the outer edges of the block.
- Fracture of the block resulted in the movement of the block lateral to the load cell wall and no significant load being recorded by the load cell wall.

The force transmission characteristics need to be considered when defining a barrier face for vehicle impact testing and when interpreting subsequent vehicle impact test results.

5.2 Mathematical Simulation

The mathematical simulation part of the study evaluated the ability of aluminium honeycomb models to predict force transmission consistent with the experimental study. This was based on predicting the load level and distribution recorded on a load cell wall behind the aluminium honeycomb model. The following can be concluded based on the simulations conducted using the continuous and discrete mesh approaches to modelling aluminium honeycomb:

- Predicted crush stress was determined by the honeycomb element stress-strain curve and for the continuous mesh model the stress-strain curve approximated a quasi-static loading. For the discrete mesh model the stress-strain curve approximated a dynamic impact at ~15.6m/s. Simulating the change in crush stress due to changes in the factors identified in the experimental study (relative density; velocity of the projectile; proportion of columns unsupported along one or more edges) would require alteration of the stress-strain curve (and additional validation data).
- The continuous and discrete mesh models predicted inaccurate load cell wall load distributions. This was due to columns bridging load cells and resulting in misappropriation of the applied load. Increasing the column density would minimise this misappropriation. Alternatively, for the discrete mesh approach aligning the columns with individual load cells would prevent misappropriation of the applied load. This would allow, within reason, for column density to be chosen based on other considerations.
- The use of beam elements with a predetermined failure load in the discrete mesh approach allowed penetration of the aluminium honeycomb to be modelled in a way that was consistent with the experimental study and without the large distortion of the surrounding material seen with a continuous mesh approach.

Based on the above a process of modification and simulation, the discrete mesh approach was selected as the preferred approach. The following can be concluded from the simulations:

- The profile of the stress-strain input curve determined the column stability and the failure pattern of the connecting beams. A change in the stress-strain curve from a 0.13MPa increase over 20% volumetric strain to a 0.07MPa increase over 80% volumetric strain resulted in column instability for the 12x12 column model when subject to uniform loading. For penetration the change to the stress-strain curve resulted in greater element strain prior to beam element failure. A balance is required to maintain column stability with increased column density and to prevent beam element failure at low element strains.
- Reducing the in-plane beam failure load resulted in a more consistent load distribution with increasing penetration. An in-plane beam failure load of 1.9kN/m resulted in a load distribution consistent with the experimental study.
- The load area bridged the centre row of load columns in the 9x9 column model resulting in an increase in the total load of 15% compared to the same load configuration using the 12x12 column model (no bridging of columns). Increasing the column density would minimise the additional deformation due to column bridging and the effect this has upon the measured load and load distribution.

It was concluded that as an analysis tool the current aluminium honeycomb models are limited in their ability to predict force transmission. These limitations need to be resolved if numerical simulation is to prove a workable alternative to experimental testing in determining vehicle crashworthiness.

References

- **Davies H, Godillon F, and Edwards M, (2004).** *Assessment of Car Compatibility Performance and the Development of Improved Compatibility.* Vehicle Safety 2004 Conference, London, UK, December 2004.
- **Gibson LJ, and Ashby MF, (1988).** *Cellular solids: Structure and properties.* Pergamon Press, New York, NY.
- **Goldsmith W, and Sackman J, (1992).** *An Experimental Study of Energy Absorption in Impact on Sandwich Plates.* International Journal of Impact Engineering, 12[2], 241-262.
- **Goldsmith W, and Louie D, (1995).** *Axial Perforation of Aluminium Honeycombs by Projectiles.* International Journal of Solids and Structures, 32, 1017-1046.
- **Hexcel Composites.** <http://www.hexcelcomposites.com>.
- **McFarland R K Jr, (1963).** *Hexagonal Cell Structures under Post-Buckling Axial Load.* AIAA Journal, 1963, 1[6], 1380-1385.
- **Mecalog Group,** Centre d'Affaires - 2 rue de la Renaissance - 92184 ANTONY cedex – France. www.radios.com
- **Ove Arup and Partners International.** EEVC Offset Deformable Barrier LS-DYNA Model – Revision 2, April 1997.
- **United Nations Regulation 94,** *Uniform Provisions Concerning the Approval of Vehicles with Regard to the Protection of the Occupants in the Event of a Frontal Collision.* <http://www.unece.org/trans/main/wp29/wp29regs81-100.html>
- **Wierzbicki T, (1983).** *Crushing Analysis of Metal Honeycombs.* International Journal of Impact Engineering, 1, 157-174.
- **Wu E, and Wu-Shung J, (1996).** *Axial Crush of Metallic Honeycombs.* International Journal of Impact Engineering, 1997, 19(5-6), 439-456.
- **Zhao H, and Gary, G (1998).** *Crushing Behaviour of Aluminium Honeycombs Under Impact Loading.* International Journal of Impact Engineering, 1998, 21[10], 827-836.

Acknowledgements

The research reported in this document was commissioned as part of the Transport Research Foundation's ongoing programme of scientific research.